JOURNAL OF PROPULSION AND POWER
Vol. 21, No. 2, March–April 2005

Design Issues in Using Integral Textile Ceramic Composites in Turbine Engine Combustors

B. N. Cox,* Q. D. Yang,† D. B. Marshall,‡ and J. B. Davis§
Rockwell Scientific Co. LLC, Thousand Oaks, California 91360

Integrally formed ceramic matrix composite structures are being developed for a range of hot-structure applications involving active cooling. Integral textile structures offer several advantages: 1) Joints between ceramic and other materials in hot zones can be avoided. 2) Thin skins (<1 mm) can be formed that are strong and tough, enabling tolerance of higher heat fluxes and the use of materials, such as oxide–oxide composites, with attractive environmental stability but relatively low conductivity and high thermal expansion. 3) Compliant structures can be designed, which can limit the development of thermal mismatch stresses. 4) Fabrication costs can be lowered by reducing part counts and steps in processing. Preliminary analyses are presented that demonstrate how these benefits might be realized for an advanced annular combustor. The possibility of a very attractive design space is indicated, based on reasonable assumptions for heat transfer coefficients for the parameter regime relevant to the new designs.

Nomenclature

A, B	=	dimensionless parameters in wall stress calculation [Eq. (18)]
A_1, A_2	=	constants in one-dimensional heat transfer model [Eq. (B3)]
a, b	=	dimensions of transpiration hole (Fig. 5a)
B_r	=	blowing ratio
C, F, G	=	constants in one-dimensional heat transfer solution [Eq. (B6b)]
c_w	=	area fraction of walls at their junction with the hot skin
$c_w E'_w/E'_h$	=	wall area fraction/compliance parameter
D	=	linear dimension
d	=	width of cavity, $r_c - r_h$
E_h, E_c, E_w	=	Young's moduli for hot skin, cool skin, and wall (or strut)
E'_h, E'_c, E'_w	=	$E_h/(1-\nu_h^2)$, $E_c/(1-\nu_c^2)$, and $E_w/(1-\nu_w^2)$
E_1, E_2, E_3	=	Young's moduli in coordinates aligned with local fiber direction
e_g, e_h	=	emissivities of combustion gas and hot skin
h_1, h_2	=	heat transfer coefficients of hot and cool surfaces of hot skin
k_c, k_b	=	stress concentration factors for compression and bending
k_f, k_s	=	thermal conductivities of fluid and solid
k_x, k_z	=	directional thermal conductivities of solid when anisotropic
L	=	separation of walls or struts
M_P, M_0	=	bending moments due to pressure drop
Q_r, Q_c	=	radiation and conduction heat fluxes
R	=	geometrical factor in 1D heat transfer model
R_c	=	radius of corner at wall/skin junction
r_h, r_c	=	radii of hot and cool skins
$r_{1/2}$	=	range of cooling influence of interior flow in transpiration hole
$T_{\text{av}}(z)$	=	temperature at depth z in hot skin averaged over skin
T_c, ρ_c, v_c, P_c	=	coolant temperature, density, velocity, and pressure
T_{op}	=	maximum operating temperature of the material
T_R	=	reference temperature (external ambient)
T_s, T_f	=	temperatures of solid and fluid in one-dimensional heat transfer model
T_1, T_2	=	temperatures of hot and cool surfaces of hot skin
T_∞, ρ_∞, v_∞, P_∞	=	freestream temperature, density, velocity, and pressure
T_1^{far}, T_2^{far}	=	temperatures of hot and cool surfaces of hot skin far from cooling influence of interior flow in any transpiration hole
$\bar{T}_{\text{hot}}$, $\bar{T}_{\text{cool}}$	=	average temperatures in hot and cool skins
t	=	thickness of generic skin
t_h, t_c, t_w	=	thicknesses of hot and cool skins and walls or struts
$t_h^{(w)}$	=	characteristic thickness for attaining simple asymptotic wall stress
u	=	coolant velocity through transpiration holes
x, z	=	in-plane and through-thickness coordinates in hot skin
α	=	coefficient of thermal expansion
β	=	Stefan–Boltzmann constant
γ	=	dimensionless parameter for bending effects [Eq. (5)]
ΔP	=	$P_c - P_\infty$
$\bar{\varepsilon}_{\text{hot}}$, $\bar{\varepsilon}_{\text{cool}}$, $\bar{\varepsilon}_{\text{wall}}$	=	average strains in the hot skin, cool skin, and wall (or strut)
η, η_∞, ζ	=	dimensionless parameters of thermal stress analysis [Eq. (3)]
λ_1, λ_2	=	constants in one-dimensional heat transfer model [Eq. (B3)]
μ	=	viscosity
ν_h, ν_c, ν_w	=	Poisson's ratio for hot skin, cool skin, and wall (or strut)
ξ, ψ	=	dimensionless parameters in temperature calculations [Eq. (9)]

Received 4 November 2002; accepted for publication 27 April 2004.

*Principal Scientist, Materials Division, 1049 Camino Dos Rios.
†Member of Technical Staff, Composite Materials Department, 1049 Camino Dos Rios.
‡Principal Scientist, Materials Division, 1049 Camino Dos Rios.
§Manager, Composite Materials Department, 1049 Camino Dos Rios.

$\sigma_c^{\text{tensile}}, \sigma_c^{\text{compressive}}$ = critical tensile and compressive stresses for hot skin

$\sigma_{\text{grad}T}, \sigma_{\text{bend}}^{(\Delta P)}, \sigma_{\text{bend}}^{(T)}$ = contributions to the maximum stress due to thermal gradients, pressure-induced bending, and temperature-induced bending

$\sigma_{\text{hot}}^{(1)}, \sigma_{\text{hot}}^{(2)}$ = maximum stresses on the hot and cool surfaces of the hot skin

$\bar{\sigma}_{\text{hot}}, \bar{\sigma}_{\text{cool}}, \bar{\sigma}_{\text{wall}}$ = average hoop stress in hot skin, cool skin, and wall (or strut)

σ_P, σ_T (or $\hat{\sigma}_T$) = pressure and temperature driving forces [Eq. (3) or Eq. (11)]

σ_1 = stress component parallel to local fiber direction

$\tau_{\text{hot}}^{(\max)}$ = maximum shear stress in the hot skin

I. Introduction

OVER the last few years, several integral structures formed by weaving ceramic fibers into complex three-dimensional configurations without significantly degrading the fibers' strength have been demonstrated.[1–3] The ability to weave three-dimensional structures, rather than two-dimensional laminates, considerably enhances the structural performance of brittle matrix composites. Whenever continuous surfaces of brittle matrix are present in a structure, as in any two-dimensional laminate, brittle delamination will place strong constraints on design. An attractive method of avoiding delamination failure in structures is to deploy fibers in all directions in which significant loads will arise, including where triaxial stresses exist, through the thickness of sheets and skins. The attachment of ceramic components to other structural materials such as superalloys is also very challenging and limits design possibilities and lifetime. Forming integral structures by three-dimensional weaving of fibers is far preferable. For example, a hot gas-facing skin can be formed integrally with walls or struts that connect it to cooler structural elements. Delamination of the skin and detachment of it from the supporting struts or walls can be eliminated as failure mechanisms by proper design. Finally, textile fabrication has been demonstrated for skins of thickness 1 mm or less.[1–3] Such fine-scale structures have not previously been available in ceramic matrix composites.

One example of an integrally woven structure relevant to turbine engine combustors is the sandwich structure shown in Fig. 1. A hot (combustion-facing) skin and a cool skin are joined by integrally woven pile yarns that can form walls dividing the space between the skins into channels. The structure is consolidated with a ceramic matrix.

The hot skin may contain an array of holes for transpiration cooling. The holes are likely to be at least 0.5 mm across to conform with current industry standards for the avoidance of blockage due to fouling. The holes can be formed during the textile fabrication process by repositioning the woven fiber tows in the hot skin. This cost-effective process can be effected without breaking or cutting fibers and, therefore, minimizes preferential damage initiation at the holes. In fact, holes formed in this way are likely not to be a significant cause of strength degradation or fatigue failure because of the very high levels of notch insensitivity possessed by textile ceramic composites.

This paper explores some design possibilities for combustors that exploit integral structures formed from ceramic fibers and matrices by weaving or other textile fabrication. The design analysis focuses on transpiring annular combustor structures. One might envisage such a component as a replacement for superalloy combustor wall liners in a conventional combustor can. However, more interesting, an integrally woven transpiring wall might be the critical component in a radical, new combustor design, such as a trapped vortex combustor.[4] (In a trapped vortex combustor, fuel and oxidizing air are held in a vortex flowfield in a cavity adjacent to the main combustor flow path until combustion is well under way and then drawn out into the freestream. The trapped vortex configuration promotes flame stability and allows a shorter overall combustor length and a reduction in the fraction of compressor air needed for cooling. Improved efficiency and reduced NO_x emissions can be achieved.) The details of the combustor design will not be addressed here. Nevertheless, conditions typical of various combustor configurations will be used to assess the potential for new designs. The possibility of a very attractive design space is indicated.

Materials of interest for integral textile combustor components include SiC–SiC and all-oxide composites. In this paper, numerical estimates are made for material properties representative of the latter group. The recent advent of two classes of tough, strong, all-oxide composites has opened new prospects for their use in turbine engine combustors. Of the two classes, one achieves damage tolerance and toughness by incorporating weak fiber/matrix interfaces that result from using monazite, for example, $LaPO_4$, as either a fiber coating or as the entire matrix[5–11] and the other by using a porous matrix of alumina and/or mullite, which may be strongly bonded to the fibers.[12–16] The fibers of most current interest for both systems are polycrystalline Al_2O_3, (Nextel® 610) or mullite/alumina (Nextel 720). Fibers of Al_2O_3/YAG (polycrystalline or eutectic) or similar alloys with superior temperature capability may become available in time.

The strength and toughness conferred by the combination of Al_2O_3 and monazite are very stable under thermal exposure. Figure 2 shows the woodlike, tough fracture mode by which a sharply notched $Al_2O_3/LaPO_4$ plain woven panel fails. Data for unidirectional Nextel 610/monazite composites exemplify the notch insensitivity of strength that is associated with such a graceful failure mechanism, even after high-temperature exposure. The retained strength following heat treatment to 1200°C for 1 h exceeds 500 MPa, which is similar to the pristine strength.[1] The Nextel fibers will degrade at higher temperatures, but the Al_2O_3/monazite interface itself is known to be stable for much longer times at temperatures up to 1600°C (Ref. 17). Because all-oxide systems are especially resistant to environmental degradation, these data encourage the expectation that high strength will survive for long lives in oxidizing environments (including those containing water vapor, which is life-limiting for SiC-based combustor components). This view is encouraged by successful 1000-h tests of porous matrix composites.[18]

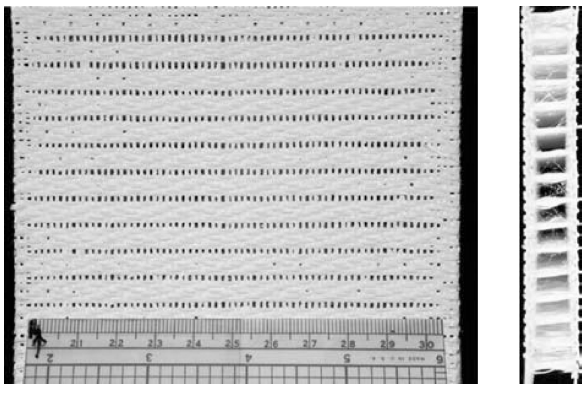

a) b)

Fig. 1 Integrally woven all-oxide transpiring structure: a) hot side and b) right edge of hot side revealing channel structure formed by pile yarns joining the hot and cold skins.

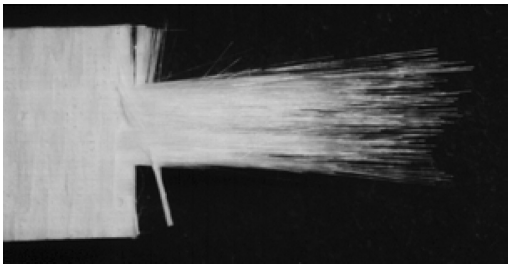

Fig. 2 Woodlike failure mode of a sharply notched bar of an $Al_2O_3/LaPO_4$ plain woven composite loaded in uniaxial tension.

Table 1 Assumed combustor conditions

Property	Symbol	Estimated value
Freestream temperature	T_∞	2500 K
Freestream pressure	P_∞	630 psi
Freestream velocity	v_∞	200 m/s
Freestream density	ρ_∞	6.3 kg/m^3[a]
Coolant temperature	T_c	1000 K
Coolant pressure	P_c	700 psi
Coolant velocity	v_c	10–30 m/s[b]
Coolant density	ρ_c	17 kg/m^3[c]

[a]Air at 2500 K.
[b]Depends on the optimum blowing ratio ($B_r = \rho_c v_c / \rho_\infty v_\infty$); $B_r \sim 0.4$ for film cooling, but much less for transpiration cooling.
[c]Air at 1000 K.

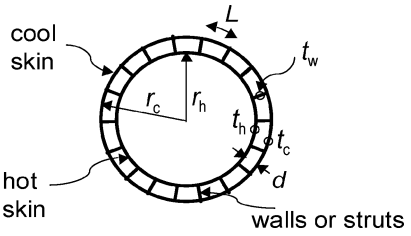

Fig. 3 Schematic of key parameters in design of integrally woven, double-skin, annular combustor wall.

II. Thermal and Mechanical Loads

Design considerations for thermal and mechanical loads will be based on the typical axisymmetric geometry shown schematically in Fig. 3, which is representative of an annular combustor. A freestream mixture of combusting gases moves across the hot (inner) skin, characterized by pressure P_∞, temperature T_∞, density ρ_∞, and velocity v_∞. Coolant is supplied via the cavity between the hot and cold skins and is characterized by pressure P_c, temperature T_c, and density ρ_c in the cavity. If transpiration holes are present, $P_\infty < P_c$ in ideal operation, so that coolant would flow out into the boundary layer through the holes. Notation for the main geometrical variables is shown in Fig. 3. The assumed combustor conditions are those shown in Table 1. They correspond to relatively high compression ratios, representative of future rather than current turbine engines. The combustion temperature $T_\infty = 2500$ K is also relatively high, especially compared to current power-generating turbines. Some results will also be presented for $T_\infty = 2000$ K, which is a more moderate combustion temperature.

Temperature and stress distributions in the combustor liner will depend on the heat flux from the combustion gases (both radiative and from turbulent conduction through the boundary layer) and the mechanisms available for cooling. The radiative component will usually appear in the design problem as a fixed, system condition: To first order, it is not affected by changes in the design of the combustor wall. Heat flux through the boundary layer via conduction depends on the difference, $T_\infty - T_1$, between the freestream temperature T_∞ and the temperature T_1 of the hot surface of the combustor wall and the heat transfer coefficient h_1 across the boundary layer. Both T_1 and h_1 are functions of location (x, y), and both are strongly influenced by design choices. Similarly, heat removal mechanisms, including direct cooling by transpiring gases, backface cooling by the reservoir of coolant (with heat transfer coefficient, h_2), solid-state heat conduction, and distributed reradiation are all subjects of design optimization.

If the hot skin contains transpiration holes, then the heat transfer coefficient h_1 between the combustion gases and the hot side of the skin is a very complicated function of many parameters, including the properties of the coolant and the freestream (density ρ, velocity v, viscosity μ, conductivity k, etc.), the flow conditions (laminar or turbulent), the temperature, and the geometry (location of holes, injection angle, surface roughness, surface curvature, etc.). In the absence of any universal relation, empirical relations for specific applications have been established and used to guide design. Unfortunately, no data are yet available for conditions that are close to those that are most attractive for transpiring hot skins fabricated by integral textile methods.

The heat transfer coefficients for the annular configuration of Fig. 3 in the absence of transpiration (upper bound for h_1) can be estimated from the Nusselt correlation (see Ref. 19),

$$Nu \equiv h_i D / k_f = 0.023 Re^{0.8} Pr^{0.4} \qquad (i = 1, 2) \qquad (1a)$$

where

$$Pr = 0.7, \qquad Re = \rho_f v_f D / \mu_f$$

$$D = \begin{cases} 2r_h & \text{(hot side)} \\ 2(r_c - r_h) & \text{(cool side)} \end{cases} \qquad (1b)$$

where ρ_f, v_f, μ_f, and k_f are the density, velocity, viscosity, and thermal conductivity of the freestream combustion or coolant fluids and r_c and r_h are the outer and inner radii of the cavity. With representative dimensions $r_h = 0.1$ m and $r_c = 0.11$ m, the value of h_1 calculated for the conditions of Table 1 is $\sim$3400 W/m$^2 \cdot$ K, whereas the range of values for h_2 is $\sim$500–1300 W/m$^2 \cdot$ K.

The net heat flux into the hot surface of the hot skin from thermal radiation, which will be important in many combustors, can be estimated from the approximate relation[20]

$$Q_r = e_g \beta T_\infty^4 [(1 + e_h)/2] \left[1 - (T_1/T_\infty)^{2.5}\right] \qquad (2)$$

where $\beta = 5.669 \times 10^{-8}$ W/m$^2 \cdot$ K^4 is the Stefan–Boltzman constant, e_g and e_h are the emissivities of the combustion gas and the hot skin. The gas emissivity is dependent on combustion chemistry, pressure, and temperature, as well as the dimensions of the combustion chamber. Typical values for hydrocarbon fuels at the conditions of Table 1 and for a combustor of diameter 0.2 m fall within the range $\sim$0.5–0.9 (Ref. 20). The emissivity of the hot skin falls within a similar range.[21] The midrange values $e_g = e_h = 0.7$ and a skin surface temperature $T_1 = 1473$ K lead to $Q_r \approx 0.3$ MW/m^2 for a freestream temperature $T_\infty = 2000$ K, and $Q_r \approx 0.9$ MW/m^2 for $T_\infty = 2500$ K. These values will be used in assessing design feasibility.

The midrange values of Q_r for $T_\infty = 2000$ K and $T_\infty = 2500$ K are 10 and 25%, respectively, of the corresponding heat flux $Q_c^{(\text{no transp})}$ due to conduction through the boundary layer in the absence of transpiration ($Q_c^{(\text{no transp})} = h_1 (T_\infty - T_1) = 3.4$ MW $\cdot$ m^2, with h_1 as estimated earlier). An upper bound for Q_r, that is, with $e_g = e_h = 1$, at $T_\infty = 2500$ K is 1.6 MW/m^2, which is about one-half of $Q_c^{(\text{no transp})}$.

III. Stress Distribution in Hot Skin

The combination of thermal strains and the pressure differential between the combustion chamber and the coolant reservoir, $\Delta P = P_c - P_\infty$, will create various stress components in the hot and cool skins and the connecting walls. Two classes of stress characteristics are of interest: 1) the distribution of spatially averaged stresses among the three components of the annular configuration, namely, the hot and cool skins and the joining walls, which are represented by the hoop stresses in the two skins, $\bar{\sigma}_{\text{hot}}$ and $\bar{\sigma}_{\text{cool}}$, and the stress component in the radial direction in the connecting walls, $\bar{\sigma}_{\text{wall}}$; and 2) local stress variations, especially through the thickness of the hot skin and in the vicinity of the skin/wall junction and transpiration holes. To reveal trends in design parameters, stress problems are solved by analytical models, for example, simple beam theory, complemented by numerical results where needed. Analytical models give accurate guides when certain restrictions are placed on the material and geometrical parameters. They are at least indicative of trends in general cases.

For analytical modeling of stresses, the hot skin will be assumed to rise from a reference temperature T_R before combustion until it sustains a uniform, linear temperature gradient through its thickness, with temperatures T_1 and T_2 on its outer and inner surfaces ($T_1 > T_2$). (These assumptions will be relaxed in subsequent sections for analyzing details of the temperature distribution.) The average temperature of the hot skin will be denoted $\bar{T}_{\text{hot}} = (T_1 + T_2)/2$.

The cool skin and the walls will be assumed both to rise to a uniform temperature $\bar{T}_{\text{cool}}$, which in most designs will be close to the temperature of the coolant T_c. (More accurately, the temperature in the walls will fall exponentially along their length from that of the inner surface of the hot skin to that of the cool skin. However, for thin walls in flowing coolant, the characteristic length of the decline is small, and the whole wall will be nearly at $\bar{T}_{\text{cool}}$.) Provided the hot skin does not buckle, the distribution of spatially averaged stresses, $\bar{\sigma}_{\text{hot}}$, $\bar{\sigma}_{\text{cool}}$, and $\bar{\sigma}_{\text{wall}}$, will depend only on the mean temperature of the hot skin, $\bar{T}_{\text{hot}}$, and not on its gradient, $T_1 - T_2$.

Assume that the system of hot and cool skins is weakly coupled to the surrounding support structure (not shown in Fig. 3) and is, therefore, free to seek its own mechanical equilibrium. (Whether this assumption is correct will depend on how the wall/skin system is attached to other support structure and, thus, coupled to the thermal expansion of that structure. Methods of weak coupling can be easily devised.) Assume further that the pressure beyond the cool skin takes the same value P_c that it has between the hot and cool skins, so that containment of the global pressure in the combustor is deferred to the surrounding support structure.

A. Average Stresses in the Skins and Walls

A simple analysis of the average strains in the components of the system for the stated average temperature distributions is presented in Appendix A. The resulting average stresses are found to be

$$\bar{\sigma}_{\text{wall}} = (1/c_w)(t_h/r_h)\{\eta\sigma_P - \eta\sigma_T\} \tag{3a}$$

$$\bar{\sigma}_{\text{hot}} = -(1-\eta)\sigma_P - \eta\sigma_T \tag{3b}$$

$$\bar{\sigma}_{\text{cool}} = -(t_h/t_c)\{\eta\sigma_P - \eta\sigma_T\} \tag{3c}$$

where

$$\sigma_P = (1-c_h)\Delta P(r_h/t_h), \qquad \sigma_T = \alpha E'_h(\bar{T}_{\text{hot}} - \bar{T}_{\text{cool}}) \tag{3d}$$

$$\eta = \zeta\eta_\infty/(\eta_\infty + \zeta), \qquad \eta_\infty = [1 + (t_h/t_c)(1 + d/r_h)(E'_h/E'_c)]^{-1}$$

$$\zeta = (r_h/t_h)(r_h/d)(c_w E'_w/E'_h) \tag{3e}$$

and E'_h, E'_c, and E'_w are defined by $E'_h = E_h/(1-\nu_h^2)$, with ν_h denoting Poisson's ratio for the hot skin, etc., and E_h, E_c, and E_w denoting Young's moduli in the hot skin, cool skin, and walls, respectively; α is the coefficient of thermal expansion, which is assumed the same for the skins and the walls; the skin thicknesses t_h and t_c and the skin separation d are defined in Fig. 3; c_w is the area fraction of the walls at their junction with the hot skin; and c_h is the area fraction of the transpiration holes in the hot skin.

In Eq. (3), the quantities σ_P and σ_T act as driving forces for stress due to the pressure difference and thermal strain mismatch. The hot skin, which is the hottest and, therefore, often the most critical part of the integral structure, bears an average compressive stress that is the sum of σ_P and σ_T weighted by the factors $1-\eta$ and η, respectively. Because $\eta_\infty > 0$ and $\zeta > 0$, $\eta < 1$ and $\bar{\sigma}_{\text{hot}} < 0$ always. The signs of $\bar{\sigma}_{\text{cool}}$ and $\bar{\sigma}_{\text{wall}}$ depend on the relative magnitudes of σ_P and σ_T.

Regimes where either σ_P or σ_T is dominant are distinguished by values of the wall area fraction/compliance parameter, $c_w E'_w/E'_h$, which is proportional to ζ. For small ζ (compliant walls), $\eta \approx \zeta$ and σ_P dominates, whereas for large ζ, $\eta \to \eta_\infty$ and σ_T dominates to an extent determined by the value of η_∞. The transition from small to large ζ can be characterized by the condition $\eta = \eta_\infty/2$, which is satisfied when $\zeta = \eta_\infty$. Because in most systems $\sigma_P \ll \sigma_T$ (Sec. V), the condition

$$c_w E'_w/E'_h < \{r_h/t_h(r_h/d) + (r_h/t_c)[(r_h/d)+1]E'_h/E'_c\}^{-1} \tag{4}$$

follows for values of the wall area fraction/compliance parameter for which significant reduction in the stress due to thermal strain will be achieved by designing compliant walls ($\eta < \eta_\infty/2$). For very compliant walls, $\bar{\sigma}_{\text{hot}}$ tends to the term proportional to ΔP; if the walls are so compliant that the skins are mechanically decoupled, the hot skin is still compressed by the pressure drop.

The results of Eq. (3) are independent of the reference temperature T_R because of the assumption that the skin/channel system is weakly coupled to the surrounding structure. Only the temperature difference $\bar{T}_{\text{hot}} - \bar{T}_{\text{cool}}$ appears, and not $\bar{T}_{\text{hot}} - T_R$, which would be much larger and, therefore, lead to larger stresses. Decoupling from the surrounding structure is, therefore, an important assumption.

B. Stress Variations in the Hot Skin

The stress in the hot skin will exhibit strong variations through the thickness of the skin, due to the temperature gradient, $T_1 - T_2$, and the bending moments generated by both the pressure drop ΔP and the average stress $\bar{\sigma}_{\text{hot}}$, acting about the skin/wall junctions. These three gradient contributions are approximately linear through the thickness of the skin and can be estimated quite accurately by beam theory. They must be superimposed on the average stress $\bar{\sigma}_{\text{hot}}$ of Eq. (3b). Their maximum values on the hot surface of the hot skin are denoted $\sigma_{\text{grad T}}$, $\sigma^{(\Delta P)}_{\text{bend}}$, and $\sigma^{(T)}_{\text{bend}}$ respectively. Further stress variations arise on the inner corner of the skin/wall junction due to stress concentration effects that are not captured by beam theory. They will be dealt with by finite element methods.

Using results derived in Appendix A, the maximum in-plane stress on the hot (upper) surface of the hot skin in the hoop direction can be written

$$\sigma^{(1)}_{\text{hot}} = \bar{\sigma}_{\text{hot}} - \sigma_{\text{grad}T} - \sigma^{(\Delta P)}_{\text{bend}} + \sigma^{(T)}_{\text{bend}} \tag{5a}$$

where $\bar{\sigma}_{\text{hot}}$ is given by Eq. (3) and

$$\sigma_{\text{grad}T} = (\alpha E'_h/2)(T_1 - T_2) \qquad \sigma^{(\Delta p)}_{\text{bend}} = \gamma\sigma_P/3 \tag{5b}$$

$$\sigma^{(T)}_{\text{bend}} = -\gamma\bar{\sigma}_{\text{hot}} \qquad \gamma = \tfrac{3}{2}(L/t_h)^2(t_h/r_h) \tag{5c}$$

with L the separation of the walls at the hot skin. Because $\bar{\sigma}_{\text{hot}} < 0$, the only positive term in Eq. (5a) is $\sigma^{(T)}_{\text{bend}}$, which for likely parameters is small, and therefore, $\sigma^{(1)}_{\text{hot}}$ is usually compressive.

A similar result can be derived for the stress on the cool surface of the hot skin at the junction of the skin and a wall, but account must also be taken here of stress concentration due to the wall/skin corner. Stress concentration factors k_c and k_b are defined for uniform in-plane (compressive) and bending loads, respectively, applied remotely to the skin. The definitions refer to the component σ_1 of tensile or compressive stress that lies parallel to the local fiber direction (axis of orthotropy) at any point near the skin/wall junction. The stress concentration factors represent the ratio of the maximum value of σ_1 to the maximum stress in the skin near but away from the junction due to either the uniform or bending load. Finite element calculations for a simple model of the wall/skin junction show that the bounds $k_c < 2$ and $k_b < 1.7$ are reasonable design limits (Appendix A).

Figure 4 shows the distribution of stress over the junction when the hot skin is loaded in bending. The zone of maximum stress concentration lies on the inner surface of the radius toward the hot

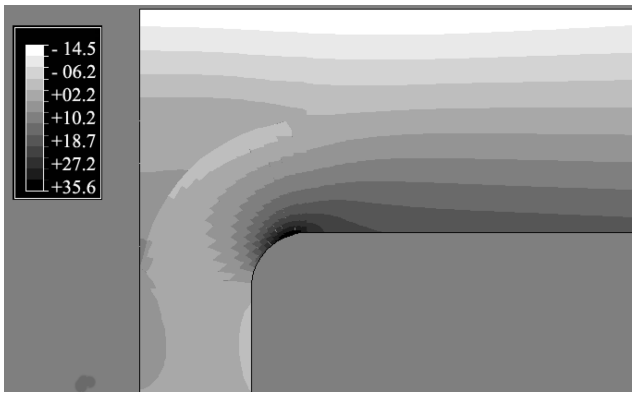

Fig. 4 Stress concentration effects at the hot skin/wall junction.

skin and is very thin: ~0.1 mm in a skin 1 mm thick. A similarly small zone of stress concentration is found when the skin or the wall is loaded uniaxially. The smallness of the stress concentration zones has strong implications for design, as discussed in Sec. VI.

When stress concentration effects are taken into account, the in-plane stress on the cool surface of the hot skin near the skin/wall junction is

$$\sigma_{\text{hot}}^{(2)} = k_c \bar{\sigma}_{\text{hot}} + k_b \sigma_{\text{grad}T} + k_b \sigma_{\text{bend}}^{(\Delta P)} - k_b \sigma_{\text{bend}}^{(T)} \tag{6}$$

which may be compressive or tensile. If it is compressive, then no tensile stress arises in the hot skin.

Equations (5) and (6) are valid only if the deflection is not large. If the deflections are large, then, for example, the nature of the divergence of $\sigma_{\text{bend}}^{(\Delta P)}$ and $\sigma_{\text{bend}}^{(T)}$ implied by Eqs. (5b) and (5c) as $t_h \to 0$ would be modified by the development of membrane stresses. (This limitation of beam theory should not be of concern in common applications.)

Shear stresses also arise in the hot skin. These can be evaluated very simply by assuming that the skin acts as a Timoshenko beam (quadratic variations of shear through the skin) and balancing the beam shears with $\bar{\sigma}_{\text{wall}}$. This results in the maximum shear stress estimate

$$\tau_{\text{hot}}^{(\max)} = (3d/4t_h)\bar{\sigma}_{\text{wall}} \tag{7}$$

where the wall may be in tension or compression. [Because of the quadratic variation of the shear stress $\tau_{zx}^{(\text{skin})}$ in Timoshenko beam theory, its maximum must be $\frac{3}{2}$ times greater than its average, which accounts for the numerical factor in Eq. (7).]

C. Stress Concentration at a Transpiration Hole

Stress concentration effects will also arise at transpiration holes. However, in this case, no meaningful estimate of the design limit seems possible without taking into account the details of the tow architecture. One design maxim, based on accumulated experience with polymeric textile composites, is that the holes should never be formed by machining and cutting fibers, but rather always by separating tows. Such tow separation or spreading creates a sphincter of concentrated reinforcement around each hole, which can lead to the periphery of the hole being stronger than the skin far from holes. The net effect is that, instead of the hole becoming a site of strain concentration and premature failure, the skin will fail elsewhere without strength knockdown. This hole-strengthening effect has been demonstrated for polymer matrix braids in Refs. 22 and 23. It is very significant in the present design problem.

In this first design analysis, transpiration holes are assumed not to create stress concentration or strength knockdown.

IV. Temperature Distribution in the Hot Skin

One principal constraint of design optimization is that the maximum temperature of the liner, which will usually be experienced on the hot surface of the hot skin, some distance away from any transpiration hole, must remain below the operating temperature of the composite material, T_{op}.

A. Direct Cooling Effect of Transpiring Coolant Flux

Even if the heat transfer coefficient h_1 is uniform across the hot surface, the temperature of the hot skin will vary because of the cooling effect of the coolant flowing out through the transpiration holes (heat flow from the surfaces of the holes to the fluid). Full analysis of this effect requires numerical modeling, for example, based on finite element methods (FEM). Figure 5a shows typical temperature distributions calculated by FEM around a square transpiration hole, assuming uniform h_1. Periodic boundary conditions have been applied, as expected for a square array of holes. Dimensional analysis shows that the temperature fields are functions of the reduced parameter set $\{k_z/h_1t_h, h_2/h_1, k_x/k_z, t_h/b, a/b, T_\infty/T_c\}$, where a and b are the dimensions marked in Fig. 5a, k_x and k_z are the in-plane and through-thickness thermal conductivities of the skin, and all other

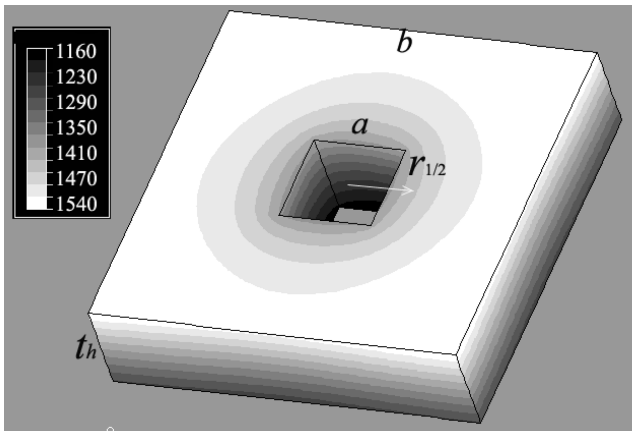

a)

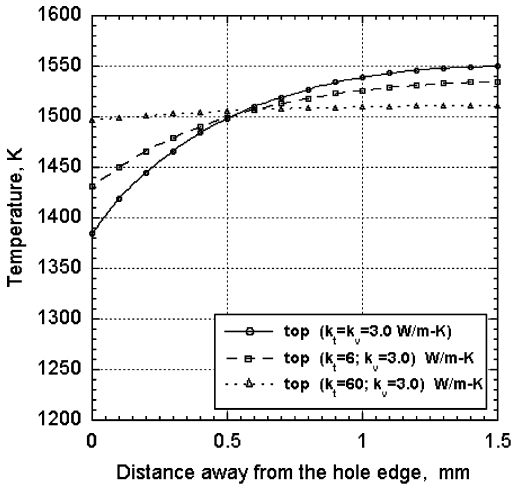

b)

Fig. 5 FEM simulations: a) temperature distributions around transpiring hole in hot skin and b) variation of the temperature of the hot surface of the hot skin with distance from the edge of a transpiring hole.

nomenclature has already been defined. In the case shown, values have been used representative of an all-oxide composite (Sec. V), namely, $T_\infty/T_c = 2.5$, $k_z/h_1t_h = 3.0$, $h_2/h_1 = 3.0$, $k_x/k_z = 1$, and $t_h/b = 0.25$. The hole spacing has been assumed to be such that $a/b = 0.25$. Figure 5a demonstrates some useful general features: 1) temperature contours become approximately circular not far from the hole, 2) the surface temperature becomes very close to uniform far from the hole, and 3) a characteristic distance $r_{1/2}$ can be defined that represents the range of influence of the hole on spatial variations of the surface temperature.

Figure 5b shows the surface temperature variation predicted by the three-dimensional model for different ratios of the thermal conductivity anisotropy, k_x/k_z. As the in-plane conductivity becomes dominant, the temperature becomes more uniform. However, the distance characterizing the range of influence of the hole varies remarkably little. Figure 5b suggests that a useful definition of $r_{1/2}$ is the distance from the center of the hole at which the surface temperature is the average of its value at the edge of the hole and its value, T_1^{far}, in the far field. This point lies approximately where the three curves almost intersect in Fig. 5b. With this definition, further simulations also show that $r_{1/2}/a$ varies weakly with k_z/h_1t_h and t_h/b. It takes values in the range $1.25 < r_{1/2}/a < 1.35$ in all cases. The single value, $r_{1/2}/a = 1.3$, will be representative for initial design studies.

For hole area fractions $c_h < 0.1$, which is the likely regime of interest, and hole widths exceeding 0.5 mm $\approx t_h$ for likely skin thicknesses, the hole separation will exceed $2r_{1/2}$, and therefore, substantial parts of the hot skin will not be cooled directly by the

transpiring fluid. An essential design boundary is, therefore, that T_1^{far} not exceed the maximum operating temperature of the composite material, T_{op},

$$T_1^{\text{far}} < T_{\text{op}} \tag{8}$$

B. Evaluation of One-Dimensional Heat Flux Models

Useful trends and limits can be obtained by a simple one-dimensional model, which has the advantage of revealing the functional dependence of the temperature distribution on design parameters in analytical form. The one-dimensional model is based on the assumption that all temperatures in the hot skin depend only on the through-thickness coordinate z. With this single assumption, temperature gradients in the z direction in both the skin and the transpiring fluid can be found. Heat transfer is considered between the skin and the fluid via the lateral walls of the transpiration holes and the top and bottom surfaces of the skin. The one-dimensional model is exact in the limits that the transpiration hole size becomes infinitesimal at fixed hole area fraction, the thermal conductivity and fluid properties are temperature independent, the solid is homogeneous, and heat transfer coefficients are uniform. Details of the one-dimensional model are presented in Appendix B.

As expected, FEM predictions of the temperature $T(z)$ through the thickness of the hot skin in the far field almost exactly coincide with those predicted by the one-dimensional model in the absence of transpiration: The cooling effect of the transpiring fluid on the lateral walls of the transpiration hole is not felt far from the hole. Figure 6 shows a comparison of the results from the one-dimensional and FEM models for $T(z)$ on the inner surface of the hole and in the far field and the function $T_{\text{av}}(z)$, which is the temperature of the skin at depth z averaged over (x, y). The temperature calculated by FEM at the hole cannot generally be estimated by the one-dimensional model; it depends on three-dimensional details of the temperature distribution. On the other hand, T_{av} predicted by the three-dimensional model is slightly higher than but close to $T(z)$ predicted by the one-dimensional model. They are close because, for a uniform heat transfer coefficient, as assumed in this simulation, the one-dimensional and three-dimensional models are satisfying very similar total heat flux conditions, which are represented in the three-dimensional model by T_{av}; the small residual difference lies in details of the temperature distribution on the inner surface of the hole. The fact that T_{av} lies so close to the temperature predicted by the one-dimensional model implies that the one-dimensional model will give quite good estimates of total heat fluxes.

The one-dimensional model becomes increasingly accurate as $k_x/k_z \to \infty$ and can even predict the temperature inside the hole to within $\pm 10^\circ$C in cases of interest when $k_x/k_z = 20$.

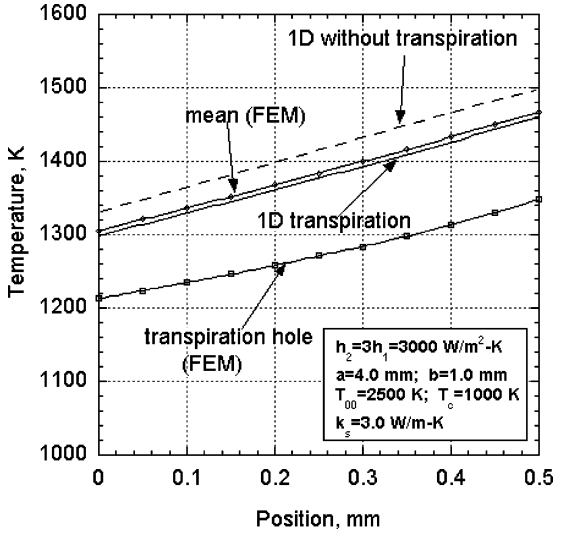

Fig. 6 Comparison of FEM calculations of the variation of temperature through the thickness of the hot skin with predictions from one-dimensional model.

C. Thermal Strains from One-Dimensional Temperature Model

A conservative approach to estimating thermal stresses is to assume that the far-field temperatures T_1^{far} and T_2^{far} prevail over the entire skin and substitute them for T_1 and T_2 in the results for thermal stresses, Eqs. (3), (5), and (6). For expected hole spacings, this will be a reasonable approximation. In this limit the one-dimensional model (Appendix B) gives

$$T_1 = \xi T_\infty + (1-\xi)T_c + \xi Q_r/h_1$$

$$\xi = [1 + h_2 t_h/k_s]/[1 + h_2/h_1 + h_2 t_h/k_s] \tag{9a}$$

$$T_2 = \psi T_\infty + (1-\psi)T_c + \psi Q_r/h_1$$

$$\psi = 1/[1 + h_2/h_1 + h_2 t_h/k_s] \tag{9b}$$

With the approximation that $\bar{T}_{\text{cool}} = T_c$, it follows that

$$\bar{T}_{\text{hot}} - \bar{T}_{\text{cool}} = \tfrac{1}{2}(\xi + \psi)[T_\infty - T_c + Q_r/h_1] \tag{10a}$$

$$T_1 - T_2 = (\xi - \psi)[T_\infty - T_c + Q_r/h_1] \tag{10b}$$

Introducing these results into Eqs. (5) and (6) leads to the following design equations for the extreme stresses in the hot skin:

$$\sigma_{\text{hot}}^{(1)} = -\sigma_P[\gamma/3 + (1-\eta)(1-\gamma)]$$
$$-(\hat{\sigma}_T/2)[\eta(1-\gamma)(\xi+\psi) + \xi - \psi] \tag{11a}$$

$$\sigma_{\text{hot}}^{(2)} = \sigma_P[k_b\gamma/3 - (1-\eta)(k_c + k_b\gamma)]$$
$$-(\hat{\sigma}_T/2)[\eta(k_c + k_b\gamma)(\xi+\psi) - k_b(\xi - \psi)] \tag{11b}$$

where

$$\hat{\sigma}_T = \alpha E_h'[T_\infty - T_c + Q_r/h_1] \tag{11c}$$

is a modified thermal driving force that includes radiative heating and all other notation has been defined in the text surrounding Eqs. (3–6). The parameters ξ and ψ depend on the heat transfer coefficients and thermal conductivity; all other parameters depend only on geometry and elastic constants.

D. Considerations of Textile Heterogeneity

Both the one- and three-dimensional models describe heat conduction through a homogeneous skin. In reality, the heat transfer problem is complicated by the textile nature of the skin material and its thermal nonlinearity. The skin is heterogeneous at the scale of the individual tows (or fiber bundles) in the textile architecture, and its thermal conductivity is sensitive to porosity and microcracking, which will evolve with temperature and stress exposure. The so-called binary model of textile composites has recently been developed to provide computationally efficient solutions to textile problems involving nonlinearity.[24–26] In a detailed design study, the binary model or other such model should be used to investigate local variations in temperature and, therefore, thermal strain. In preliminary design studies, the assumption of homogeneity is acceptable.

V. Design Estimates for All-Oxide Combustor Walls

Design estimates will now be developed using the properties shown in Table 2 for a representative $Al_2O_3/LaPO_4$ composite of Nextel 610 fibers in a monazite matrix, with weak interfaces. Tensile strength values have been measured in macroscopic coupons. Compressive strengths have been estimated roughly in the absence of firm data. Similar property values have been measured in oxide composites that are toughened via porous matrices[14] and in SiC–SiC composites,[27] the latter having significantly higher thermal conductivity, but shorter lifetimes in oxidizing combustion environments. These property data must in time be developed into statistical distributions and complemented with fatigue and creep data, before engineering design allowables can be established. They are used

Table 2 Properties of $AI_2O_3/LaPO_4$ composite

Property	Symbol	Estimated value
Tensile strength	$\sigma_c^{\text{tensile}}$	250 MPa[a]
Compressive strength	$\sigma_c^{\text{compressive}}$	250 MPa[b]
In-plane modulus	E	100 GPa[a,c]
In-plane thermal expansion	α	9×10^{-6} K^{-1}
Through-thickness thermal conductivity	k_s	3–6 W/m · K
Maximum operating temperature	T_{op}	1200°C

[a]For 0/90 deg plain woven laminate with approximately equal loadings of warp and weft fibers and total fiber volume fraction of 40% (Ref. 1). Strengths approximately twice this have been measured for unidirectional composites.
[b]Estimated value for local compressive failure by kink band formation in a constrained small volume in the hot skin (~1 mm^3 or less).
[c]Slightly increased modulus on achieving greater matrix densification.

here in the spirit of exploring new concepts in an initial feasibility study.

Although correlations suggest that the hot-side heat transfer coefficient might be near 3000 W/m^2 · K in the absence of transpiration cooling (Sec. II), data in the presence of transpiration do not exist. To inform the present assessment of design concepts, estimates will, therefore, be made of the range of values of h_1 that are required to achieve sustainable thermal strains and material temperatures. The required values of h_1 will be seen to seem feasible, but the transpiration fluxes required to achieve them must be determined elsewhere.

A. Conditions for Assuring $T_1 \leq T_{\text{op}}$

The maximum operating temperature of the composite, T_{op}, sets a practical upper bound for T_1, the temperature of the hot surface of the hot skin. Because this must be a fixed limit in any application, design rules can be deduced by imposing the constraint $T_1 \leq T_{\text{op}}$. From Eq. (9a), this constraint implies that h_1 must satisfy

$$h_1(T_\infty - T_{\text{op}}) \leq \frac{h_2(T_{\text{op}} - T_c)}{1 + h_2 t_h / k_s} - Q_r \tag{12}$$

When it is observed from Eq. (9) that $(T_1 - T_c)/(T_2 - T_c) = 1 + h_2 t_h / k_s$, this condition can be recognized as the conservation of flux, rewritten to replace T_2 by controllable parameters. Because the right hand side of Eq. (12) must be positive, constraints are implied on h_2 and the ratio k_s/t_h. One must have

$$h_2 > Q_r / [(T_{\text{op}} - T_c) - Q_r t_h / k_s] \tag{13a}$$

$$(k_s/t_h)(T_{\text{op}} - T_c) > Q_r \tag{13b}$$

Equation (13b) defines a maximum allowable skin thickness in the limit where h_1 is reduced to zero by transpiration (only radiation to be dealt with) and the Biot modulus $Bi = h_2 t_h / k_s$ is large enough to saturate the backface cooling ($T_2 \to T_c$). Less effective transpiration or backface cooling would require a thinner skin. With parameters from Tables 1 and 2 ($T_\infty = 2500$ K, $T_{\text{op}} = 1473$ K, $T_c = 1000$ K, and $k_s = 4$ W/m · K) and the midrange value of Q_r from Sec. II ($Q_r = 0.9$ MW/m^2), the maximum skin thickness allowed by Eq. (13b) is ~2.1 mm. With the upper bound radiation level $Q_r = 1.6$ MW/m^2 (Sec. II), the maximum thickness is reduced to ≈1.2 mm.

For any skin thickness less than this maximum, the condition of Eq. (13a) defines the minimum required value of h_2 to deal with the radiation flux alone, that is, when h_1 is assumed to be zero. The condition on h_2 can be satisfied by controlling the Reynolds number and mass flux of the coolant between the hot and cool skins. With the same temperatures and conductivity, a skin of thickness 1 mm, for example, would require $h_2 > 700$ W/m^2 · K for $Q_r = 0.3$ MW/m^2 and $h_2 > 1.2 \times 10^4$ W/m^2 · K for $Q_r = 1.5$ MW/m^2. Although the latter, extreme radiation level is unlikely to be encountered, these results highlight the potential sensitivity of the design boundary to radiation.

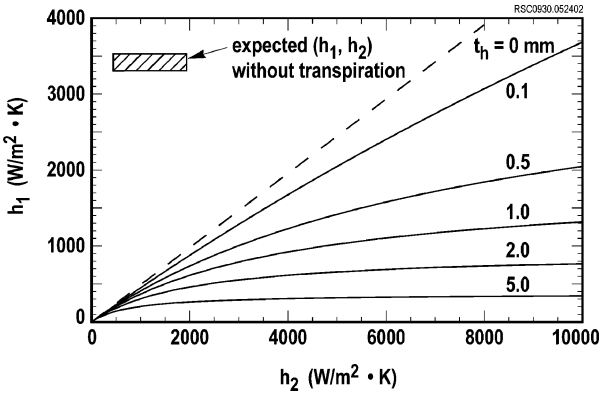

Fig. 7 Maximum admissible value of h_1 for one representative set of design parameters as function of cool-side heat transfer coefficient h_2 and skin thickness t_h.

When Eq. (13) has been satisfied, Eq. (12) implies a target value for h_1, which may or may not imply the necessity of transpiration cooling. Figure 7 shows the limiting value of h_1 as a function of h_2 for several skin thicknesses t_h with the same temperatures and conductivity and $Q_r = 0$ (no radiation). For $t_h < 1$ mm and h_2 in the range 500–1300 W/m^2 · K (from Sec. II), values of h_1 in the range 250–550 W/m^2 · K are sought. This range lies well below the value of h_1 estimated in Sec. II in the absence of transpiration (3400 W/m^2 · K). Thus, for relatively high combustion gas temperatures, $T_\infty \sim 2500$ K, transpiration cooling must play a key role in the combustor design. When $T_\infty = 2000$ K, with all else fixed, the allowed values of h_1 approximately double, but transpiration is still required.

Radiative heating will further reduce the target value of h_1, by the amount $Q_r/(T_\infty - T_{\text{op}})$. For the midrange radiation level, $Q_r = 0.3$ MW/m^2 (rough estimate in Sec. II for $T_\infty = 2000$ K), this reduction in h_1 is 300 W/m^2 · K. For $Q_r = 0.9$ MW/m^2 (corresponding to $T_\infty = 2500$ K), the reduction is 900 W/m^2 · K. To ensure that a feasible value results for h_1, lower skin thickness, $t_h < 1$ mm or higher h_2 may have to be achieved, with the required improvements quite strongly dependent on T_∞.

B. Thermal and Mechanical Stress

Here the total stress in the hot skin at the wall/skin junction, $\sigma_{\text{hot}}^{(1)}$ and $\sigma_{\text{hot}}^{(2)}$, will be analyzed as a function of the skin thickness t_h. Unless otherwise stated, the cool-side heat transfer coefficient h_2 is assigned the value $h_2 = 1000$ W/m^2 · K; the wall area fraction/compliance parameter $c_w E_w'/E_h'$ is assigned the value 10^{-3}, which could correspond to a wall area fraction $c_w = 0.01$, and an effective wall stiffness that is 1/10th the stiffness of the hot skin; and geometrical parameters are assigned the values $t_c = 1$ mm, $r_h = 100$ mm, $d = 10$ mm, and $L = 10$ mm. Temperatures are as stated in Table 1; thus the high value $T_\infty = 2500$ K is used. The hot-side heat transfer coefficient h_1 is determined by the limit of Eq. (12), that is, it is assigned the value that leads to $T_1 = T_{\text{op}} = 1473$ K = 1200°C in the one-dimensional heat model. Thus, h_1 is not a constant, but varies with t_h. The hot and cool skins have equal Young's moduli.

With the constraint that $T_1 = T_{\text{op}}$, the total heat flux $[Q_r + h_1(T_\infty - T_c)]$ and the temperature distribution in the skin are fixed for given values of all other parameters [Eq. (12)]. Therefore, there is no distinction between the effects of radiative heating and conduction through the boundary layer on the computed stresses. Equation (10) shows that, to maintain $T_1 = T_{\text{op}}$, Q_r and h_1 will change in such a way that $(\xi + \psi)[T_\infty - T_c + Q_r/h_1]$ and $(\xi - \psi)[T_\infty - T_c + Q_r/h_1]$ remain fixed, and therefore, the stresses in Eq. (11) remain fixed.

Figure 8 shows the variations of contributions to the maximum stress found on the hot surface of the hot skin, which can be separated into thermal stresses and stresses caused by the gas pressure drop Δp. The thermal stresses can be further decomposed into a stress arising from the average temperature in the hot skin,

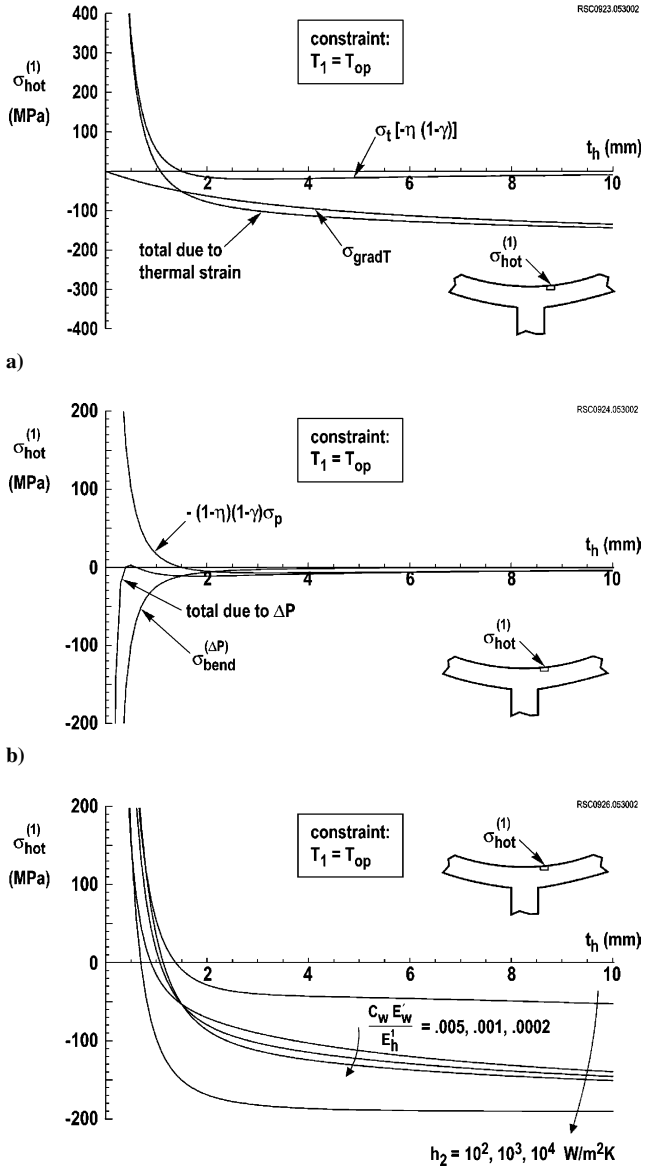

Fig. 8 Stress contributions to the maximum stress on the hot surface of the hot skin: a) thermal stresses, b) stresses due to gas pressure drop, and c) total stress.

$-\eta(1-\gamma)(\xi+\psi)\hat{\sigma}_T/2$, and one due to the temperature gradient, $-(\xi-\psi)\hat{\sigma}_T/2$ (Fig. 8a).

The stress arising from the average temperature in the hot skin can be controlled by ensuring that the structure is compliant, that is, by minimizing the wall area fraction/compliance parameter, $c_w E'_w/E'_h$ (and, therefore, η). For small $c_w E'_w/E'_h$, the stress due to the average temperature in the hot skin is approximately proportional to $c_w E'_w/E'_h$ [Eq. (3)].

The stress contribution due to the temperature gradient vanishes when $t_h \to 0$ because $T_2 - T_1 \to 0$ and, therefore, the factor $\xi - \psi \to 0$. For a material with a high coefficient of thermal expansion, such as an all-oxide composite, this is a strong design driver toward thin skins, for example, $t_h < 1$ mm. However, as $t_h \to 0$, the factor $1-\gamma$, which is associated with bending effects, becomes dominant, and the contribution due to the average skin temperature becomes positive ($1-\gamma \to -\gamma$) and diverges. The optimum skin thickness is found as a compromise between minimizing thermal gradient and bending effects.

When $t_h \to \infty$, $\eta \propto 1/t_h$, $\gamma \to 0$, $\xi \to 1$, and $\psi \to 0$; therefore, the stress due to the temperature gradient becomes asymptotically constant, whereas that due to the average temperature vanishes. For small t_h, the stress due to the thermal gradient is linear in t_h,

$$\sigma_{\text{grad}T} \approx (\alpha E'_h/2)(h_2 t_h/k_s)[1 + h_2/h_1][T_\infty - T_c + Q_r/h_1] \quad (14)$$

The vanishing of $\sigma_{\text{grad}T}$ as $t_h \to 0$ can be traced through Eq. (10b) to vanishing of the temperature gradient ($T_1 \to T_2$). Because thermal stresses due to the temperature gradient can be limited by choosing t_h to be small, one design goal should be to mitigate bending effects, by reducing the wall spacing or by innovative integral structure design, so that they remain modest for the thinnest skins that can be fabricated.

Figure 8b shows the stress due to the pressure drop, ΔP, decomposed into contributions due to the average stress in the hot skin, $-(1-\gamma)(1-\eta)\sigma_P$, and the bending moment generated by Δp about the skin/wall junction, $-\gamma\sigma_P/3$. Both contributions diverge as $t_h \to 0$ because both contain bending effects, but with opposite signs. Both contributions diminish in magnitude as $t_h \to \infty$, the former as t_h^{-1} and the latter as t_h^{-2}. In general, the stresses due to ΔP are significant only in setting a lower bound to t_h. No simple analytical result is available for the bound, but it will probably always be substantially less than 1 mm for parameters of interest. Once again, designs that mitigate bending effects will be helpful.

Figure 8c shows the total stress (sum of thermal stress and mechanical stress) at the hot surface of the hot skin as a function of t_h. Two families of curves are shown, illustrating the dependence of $\sigma^{(1)}_{\text{hot}}$ on the assumed heat transfer coefficient h_2 and the wall area fraction/compliance parameter $c_w E'_w/E'_h$. The parameter $c_w E'_w/E'_h$ has a significant effect over a range of values of interest for t_h. Because the heat transfer coefficients are very uncertain, the generous range 100–10,000 W/m$^2 \cdot$K has been considered for h_2, with significant resulting variation in $\sigma^{(1)}_{\text{hot}}$, but with a range of values of t_h always available for which the magnitude of $\sigma^{(1)}_{\text{hot}}$ is acceptable.

The total stress $\sigma^{(1)}_{\text{hot}}$ changes sign at some value of t_h. Therefore, there is an optimal range of values of t_h for which the magnitude of the stress is small. A simple algebraic expression for the limits of this domain cannot be found. [They are related nontrivially to the characteristic values of Eq. (14).] Inspection of Eqs. (11) and (13) shows that they depend on the wall area fraction/compliance parameter, thermal parameters, and geometrical dimensions.

Figure 9a shows the contributions to the maximum stress expected on the cool side of the hot skin (near the wall/skin junction), following Eq. (11). The same contributions arise as for the stress on the hot side of the skin, but added together with stress concentration factors and different signs. A significant compressive stress arises for small values of t_h, traceable to the bending moment due to the combination of the average compressive stress in the hot skin and its curvature, $\sigma^{(T)}_{\text{bend}}$. Figure 9b shows the total stress $\sigma^{(2)}_{\text{hot}}$, which can be either tensile or compressive, depending on the skin thickness. Families of curves illustrate the dependence on h_2 and the wall separation L. Because of the strength of the bending stress, $\sigma^{(T)}_{\text{bend}}$, the range of skin thickness t_h for which the magnitude of the stress $\sigma^{(2)}_{\text{hot}}$ is small is somewhat greater than for $\sigma^{(1)}_{\text{hot}}$. Both h_2 and L have significant effects on the limits of the design range of t_h.

For the material strength expected for an all-oxide composite and with the assumption that the heat transfer coefficients are attainable, a feasible design space (sustainable stress values) in which both $\sigma^{(1)}_{\text{hot}}$ and $\sigma^{(2)}_{\text{hot}}$ have acceptable magnitudes exists for hot-skin thickness in the approximate range $1 < t_h < 3$ mm. However, the required value of h_1 becomes significantly smaller and, therefore, any required transpiration coolant flux becomes greater as t_h increases [Eq. (12)], while more stringent restrictions are placed on the sustainable radiative heating flux [Eq. (13a)]. Therefore, there will always be advantage in reducing t_h as far as stress considerations allow. The key to reducing t_h is to minimize bending effects.

C. Buckling of the Hot Skin

Because the hot skin is in compression, it can buckle, which might be considered a mechanism of failure or alternatively a deliberate design condition for reducing the average compressive stress $\bar{\sigma}_{\text{hot}}$. To first order, the critical condition for buckling depends on the

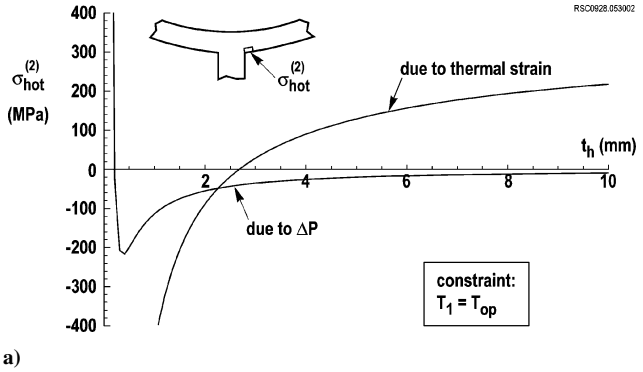

a)

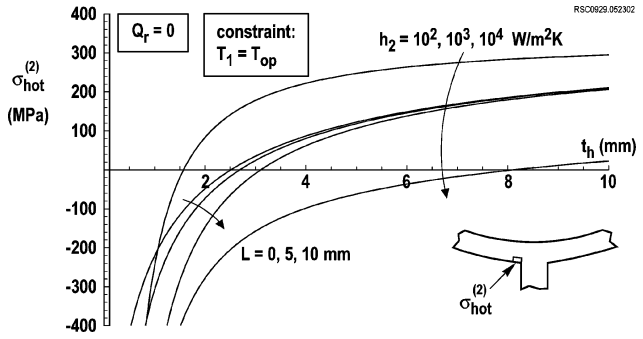

b)

Fig. 9 Stress contributions to the maximum stress on cool surface of the hot skin: a) thermal stress and stress due to gas pressure drop, and b) total stress.

average stress $\bar{\sigma}_{\text{hot}}$ only and not on the bending moments due to the pressure drop ΔP and the thermal gradient, $T_1 - T_2$. Assume that the walls are stiff enough that deflections are zero at successive wall joints. If the wall separation L is much less than r_h, the curvature of the segment has a small effect and the Euler buckling condition for a flat plate is appropriate.[28] For given hot $\bar{\sigma}_{\text{hot}}$ a critical value of the skin thickness will separate buckling and nonbuckling behavior,

$$t_h/L > \left(\sqrt{3}/\pi\right)\sqrt{-\bar{\sigma}_{\text{hot}}/E'_h} \qquad (\bar{\sigma}_{\text{hot}} < 0) \tag{15}$$

With Eqs. (3b) and (10a), this yields the design constraint to avoid local buckling that

$$t_h/L > \left(\sqrt{3}/\pi\right)\sqrt{(1-\eta)(1-c_h)(\Delta P/E'_h)(r_h/t_h) + (\eta\alpha/2)(\xi+\psi)[T_\infty - T_c + Q_r/h_1]} \tag{16}$$

Under the constraint that h_1 satisfies $T_1 = T_{\text{op}}$, this condition can be assessed by choosing a value of t_h, finding h_1 and, thus, the state of stress in the hot skin, and using Eq. (16) to predict the minimum value $t_h^{(b)}$ of t_h required to suppress buckling under this stress state. The results of such a calculation for the same parameter set defined earlier are shown in Fig. 10. Local buckling can be expected when the curve for $t_h^{(b)}$ lies above the line $t_h^{(b)} = t_h$. For the case considered, the buckling domain is restricted to $t_h < 0.3$ mm. Nevertheless, local buckling is obviously possible for other feasible design choices; it may even be desired as a mechanism for relieving compressive stresses in the hot skin. This effect can be augmented by designing the skin with an initial deflection. Finite element calculations show that creating an initial deflection of amplitude $L/10$ reduces the maximum compressive stress on the hot surface of the hot skin by approximately 25% and imposes a substantial additional tensile load on the cool side of the hot skin. Because $\sigma_{\text{hot}}^{(2)}$ is compressive as t_h decreases and small t_h is desirable for thermal management, a deflected design may be beneficial; however, any benefit is best evaluated by three-dimensional analysis when other design parameters have been set.

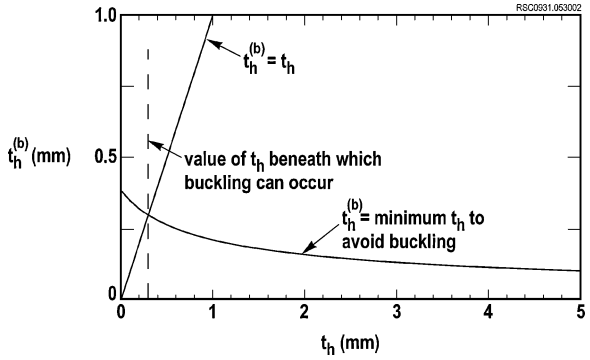

Fig. 10 Mimimum hot-skin thickness to avoid local buckling, given stress state predicted under the constraint that $T_1 = T_{\text{op}}$.

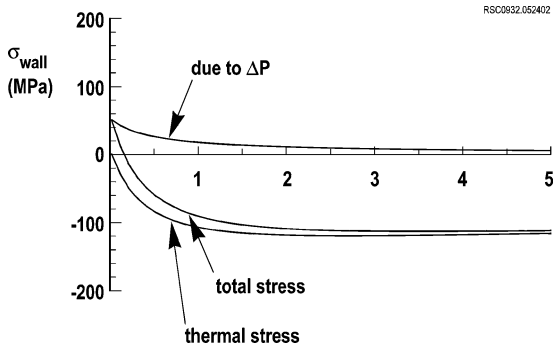

Fig. 11 Stress in walls.

D. Wall Failure

The stress in the wall follows from Eqs. (3a) and (9) as

$$\bar{\sigma}_{\text{wall}} = (1/c_w)(t_h/r_h)\{\eta(1-c_h)\Delta P(r_h/t_h) - \eta\alpha[(\xi+\psi)/2](T_\infty - T_c + Q_r/h_1)E'_h\} \tag{17}$$

This function and its decomposition into contributions from the pressure drop ΔP and the thermal strains are plotted in Fig. 11 for the same set of design parameters as used earlier and with the constraint that $T_1 = T_{\text{op}}$. As $t_h \to \infty$, only the thermal strain creates significant stress, and this approaches the asymptote

$$\bar{\sigma}_{\text{wall}} \to -\frac{\alpha E'_h(T_\infty - T_c + Q_r/h_1)}{2c_w}\frac{AB}{A+B} \qquad (t_h \to \infty)$$
$$A = \frac{r_h}{h}\frac{c_w E'_w}{E'_h} \qquad B = \frac{t_c}{r_h + h}\frac{E'_c}{E'_h} \tag{18}$$

When $t_h \to 0$, the component due to the pressure drop tends to $(1-c_h)\Delta P/c_w$, while the component due to thermal stress tends to the asymptotic form

$$\bar{\sigma}_{\text{wall}} \to -[\alpha E'_h(T_{\text{op}} - T_c)/c_w](t_h/r_h) \tag{19}$$

The asymptotic limit is approached when t_h exceeds a characteristic value given by

$$t_h^{(w)} = \frac{r_h}{2}\frac{T_\infty - T_c}{T_{\text{op}} - T_c}\frac{AB}{A+B} \tag{20}$$

The stress in the wall is compressive for all cases of interest.

E. Local Cracking

A further design question beyond the scope of this paper is whether microcracking and spalling might occur in small volumes of material near features that give rise to severe thermal gradients. One such location is the inner surface of a transpiration hole, where the cooling effect of the transpiring fluid tends to cause hoop tension. Whereas excellent resistance to spalling has been demonstrated for textile composite rocket nozzle liners[3] where thermal gradients are $\sim 2000^{\circ}\mathrm{C/mm}$, whether spalling is suppressed in each new case will depend on small details of the textile design. This question is the subject of current research.

VI. Discussion

A. Design Feasibility

The feasibility of a design space has been demonstrated, based on using the integral textile approach to creating a compliant structure. Among the benefits of integral textile forming are that thin skins and compliant structures can be achieved without compromising strength or integrity.

Achieving thin skins is important for sustaining high thermal flux loading and for controlling thermal stresses due to the temperature gradient in the hot skin. For oxide–oxide composites, Fig. 7 suggests that, for likely cool-side heat transfer coefficients and total heat fluxes, a hot-skin thickness less than 1 mm is desirable. Equation (14) suggests that a similar skin thickness is required to control thermal stresses due to the temperature gradient.

Fabricating a compliant structure minimizes the thermal stresses due to the average temperature in the hot skin, which are approximately proportional to the area fraction/compliance parameter $c_w E'_w/E'_h$. For all-oxide composites, $c_w E'_w/E'_h < 10^{-3}$ is desirable and achievable.

The feasibility of maintaining a given material below its allowable operating temperature T_{op} depends on the values of heat transfer coefficients. Unfortunately, while a large body of literature reports the effectiveness of film and transpiration cooling for rocket and industrial engines (e.g., Refs. 29–34), none of the data have been acquired under conditions that are representative of the novel annular combustors that have been considered here. Data depend strongly on parameters such as the testing temperature, the blowing ratio, and the geometry of the cooled skin, including the transpiration holes. Some data on film cooling and transpiration through porous media suggest that values of h_1 with order of magnitude in the range 100–1000 $\mathrm{W/m^2 \cdot K}$ might be attained in a relevant combustor configuration. If so, the design estimates provided here for temperature and thermal strain management will be approximately correct.

The considerations of Sec. V. A show that the maximum combustion temperature at which an all-oxide composite might be used without exceeding the material operating temperature will be limited by radiation heat flux. For the highest combustion temperature considered, $T_\infty = 2500$ K, aggressive schemes may be required to increase backface cooling (raising h_2), by changing the geometry or the coolant flux, or else the skin thickness must be reduced well below 1 mm. The feasibility of either of these approaches is questionable. For lower T_∞, for example, $T_\infty = 2000$ K, the problem appears more easily managed.

An essential remaining issue is the question of how much cooling air will be required to attain workable values of h_1 in a combustor. Only the acquisition of relevant data will resolve this question and, thus, determine the system advantages of ceramic components.

B. Mitigation of Bending Stresses

Figures 8 and 9 show that, for the geometry chosen for this initial design assessment, stresses of diverging magnitude limit the minimum allowable skin thickness t_h to values of 1 mm or more. Inspection of Eqs. (3), (5), and (6) reveals that all large stresses at small t_h, whether originating in the average temperature in the hot skin, or the temperature gradient through the hot skin, or the gas pressure drop, arise from bending effects about the skin/wall junction. The bending effects are a serious challenge for design: Optimizing the heat transfer problem and minimizing stresses due to thermal gradients lead to the desire for skins that are as thin as possible. In weight critical applications, such as aircraft engines, weight optimization points the same way.

The bending effects depend strongly on the geometry of the junction, as well as the heterogeneity and anisotropy of the textile material from which the junction is formed. One approach to reducing bending effects is to reduce the wall spacing L; the bending parameter γ varies as L^2 [Eq. (5c)]. However, reducing L increases the area fraction of the walls and, therefore, the area fraction/compliance parameter $c_w E'_w/E'_h$, which is undesirable.

A superior approach to mitigating bending effects is to change the geometry of the walls. The square shape (with rounded corners) assumed here is in fact unfavorable for bending. Other configurations, such as walls or struts that join the hot skin obliquely, reduce or virtually eliminate bending stresses. Part of this reduction can be attributed to reduction of the effective wall modulus E'_w and part to reduction of the stress concentration factor k_b. Further improvements can be expected from the textile nature of the proposed structures. The trick in avoiding bending stress concentrations is to carry loads in the walls and the skin by separate fiber bundles (tows), while integrating the walls and the skin with relatively few fibers woven in the through-thickness direction. Such textile architecture will be demonstrated elsewhere. With bending effects strongly reduced, the design option of very thin skins, for example, <1 mm, is opened. The present study highlights the importance of getting the wall/skin architecture right.

C. Nonlinear Problem in Many Variables

The optimization problem is an interesting challenge because the problem of heat transfer with transpiration-modified boundary layers must be coupled to the problems of calculating heat conduction through the textile structure and thermal and mechanical stresses in a part in which many geometrical features can be varied in shape and dimension. Simultaneous account must be taken of thermal strains, mechanical loads, heat transfer coefficients, total required coolant flux, radiation, preform architecture, and part geometry. All of these factors are related to one another in complicated, nonlinear ways.

The heat transfer coefficients (and, therefore, the thermal fluxes) depend on the sizes of interior cavities in the proposed double skin structure and the gross dimensions of the combustor liner; for example, for an annular cavity with a turbulent flow, the cool-side heat transfer coefficient h_2 can be estimated from Eq. (1), which indicates that h_2 can be raised (which is desirable) by reducing the gap, $d = r_c - r_h$, between the skins, or by increasing v_c. The dependence of h_2 on $r_c - r_h$ in Eq. (1) is weak, with $h_2 \propto (r_c - r_h)^{-0.2}$; however, the joint dependence of h_2 on v_c and $r_c - r_h$ introduces the possibility of adjusting h_2 at a fixed value of the coolant mass flux.

Although the heat transfer coefficients depend on the geometry of the integral structure, the maximum allowed thermal and mechanical stresses set separate bounds on the hot-skin thickness and other dimensions. Design optimization for thermal strains consists of solving the coupled nonlinear equations governing stresses [Eq. (11)] and heat transfer coefficients, for example, Eq. (1), subject to the constraints of the maximum material operating temperature and system requirements, such as the maximum coolant flux. Simultaneously, system requirements, especially limitations on the available coolant flux, set bounds on the achievable reductions of heat transfer by transpiration, while the maximum allowable hot-skin thickness depends on the heat fluxes and the maximum material operating temperature.

The elementary results for temperature distributions and thermal and mechanical stresses that have been presented here provide a partial solution to a rich and complex optimization problem. Optimization for novel combustor configurations such as the trapped vortex combustor remains a fascinating challenge.

D. Textile Mechanics and Size-Scale Effects

A second important issue in assessing the design limits imposed by bending stresses at the junction is that the maximum stresses extend over quite small volumes. Small volumes of ceramic composites are known to exhibit strengths that may be two to three times

those of standard coupons.[35,36] In tensile tests, for example, strains of 2–2.5% have been measured over gauge lengths ~0.2 mm at notch roots in specimens of woven C/SiC composites, whereas unnotched specimens of the same material fail at macroscopic strains ~1% (Ref. 36). The ratio of the maximum local stress to the macroscopic failure stress is believed to be similar to that of the strains. Such a gain in strength relative to coupon data would be especially significant in dealing with the bending stress concentrations. Test data, including fatigue and creep data, will decide this question.

Size-dependent strength criteria must be applied to stresses or strains calculated on the relevant scale, which will be of the same order as the tow width in the textile reinforcement. A textile model such as the binary model is required to calculate local strains in complex textile architectures.[24–26]

VII. Conclusions

Simple design estimates have been presented for an annular combustor, which show how material and geometrical design choices control the design envelope. The possibility of a very attractive design space for advanced combustors based on integrally formed ceramic matrix composite structures has been indicated. Key enabling attributes include avoiding joints between dissimilar hot materials, the ability to make robust yet very thin skins (<1 mm), minimization of thermal stresses through the use of compliant structures, and possibly low fabrication costs.

Appendix A: Thermal and Mechanical Stresses in an Annular Configuration

Equilibrium and displacement continuity conditions for the annular configuration of Fig. 3 may be stated as follows. Consider first the forces acting on one-half of the hot skin regarded as a free body (Fig. A1a), namely, tractions on the sections of the skin equal in magnitude to the hoop stresses, the pressure drop ΔP acting around the outer surface of the skin, and the axial stresses in the walls, which act as normal tractions on the outer surface.

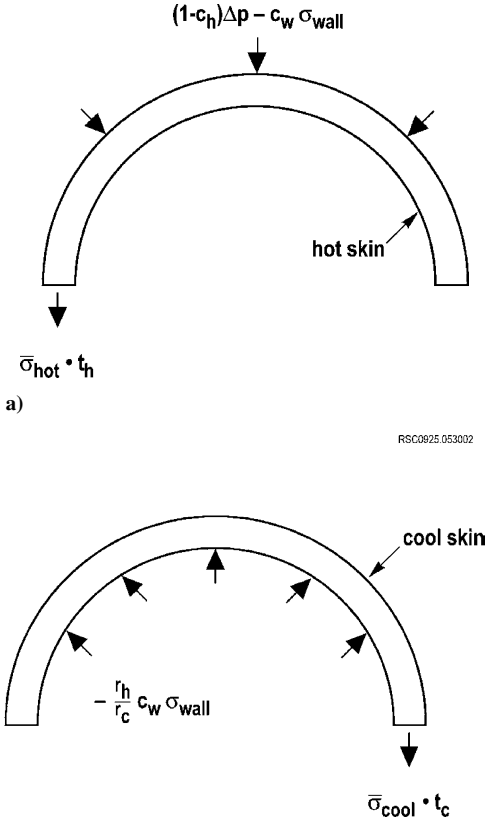

Fig. A1 Free-body diagrams used to analyze average stresses in hot and cool skins and walls.

Spatially Averaged Stresses

If the walls are sufficiently numerous, their effect can be represented as a continuous pressure, $c_w\bar{\sigma}_{\text{wall}}$, where c_w is the area fraction of the walls on the outer surface of the hot skin. Denote by wall $\bar{\varepsilon}_{\text{wall}}$, $\bar{\varepsilon}_{\text{hot}}$, and $\bar{\varepsilon}_{\text{cool}}$ the total average strains in the walls and hot and cool skins, respectively. Then under plane strain conditions,

$$\bar{\sigma}_{\text{hot}} = E'_h(\bar{\varepsilon}_{\text{hot}} - \alpha\Delta T_h) \tag{A1a}$$

$$\bar{\sigma}_{\text{cool}} = E'_c(\bar{\varepsilon}_{\text{cool}} - \alpha\Delta T_c) \tag{A1b}$$

$$\bar{\sigma}_{\text{wall}} = E'_w(\bar{\varepsilon}_{\text{wall}} - \alpha\Delta T_c) \tag{A1c}$$

where $\Delta T_h = \bar{T}_{\text{hot}} - T_R$, $\Delta T_c = \bar{T}_{\text{cool}} - T_R$, and the other nomenclature is already defined. Equilibrium of the forces acting on the free body requires

$$\int_{-\pi/2}^{\pi/2} [c_w E'_w(\bar{\varepsilon}_{\text{wall}} - \alpha\Delta T_{\text{cool}}) - (1 - c_h)\Delta P] r_h \cos\theta \, \mathrm{d}\theta = 2E'_h(\bar{\varepsilon}_{\text{hot}} - \alpha\Delta T_{\text{hot}})t_h \tag{A2}$$

A similar construction for half of the cool skin regarded as a free body (Fig. A1b) leads to

$$\int_{-\pi/2}^{\pi/2} \frac{r_h}{r_c} c_w E'_w(\bar{\varepsilon}_{\text{wall}} - \alpha\Delta T_{\text{cool}}) r_c \cos\theta \, \mathrm{d}\theta = -2E'_c(\bar{\varepsilon}_{\text{cool}} - \alpha\Delta T_{\text{cool}})t_c \tag{A3}$$

where the product $r_h c_w / r_c$ equals the area fraction of the walls on the inner surface of the cool skin (assuming the walls have constant thickness). A third condition on the three unknown strains arises from continuity of displacements,

$$(1 + \varepsilon_{\text{cool}})r_c - (1 + \bar{\varepsilon}_{\text{hot}})r_h = (1 + \bar{\varepsilon}_{\text{cool}})(r_c - r_h) \tag{A4}$$

Equations (A2–A4) can be solved for $\bar{\varepsilon}_{\text{wall}}$, $\bar{\varepsilon}_{\text{hot}}$, and $\bar{\varepsilon}_{\text{cool}}$, and some manipulation yields

$$\bar{\varepsilon}_{\text{wall}} = \alpha\Delta T_c + [(1 - c_h)(r_h/t_h)(\Delta P/E'_h) - \alpha(\bar{T}_{\text{hot}} - \bar{T}_{\text{cool}})](r_h/h)[1/(1 + \chi)] \tag{A5a}$$

$$\bar{\varepsilon}_{\text{hot}} = \alpha\Delta T_h - (1 - c_h)(r_h/t_h)(\Delta P/E'_h) + [(1 - c_h)(r_h/t_h)(\Delta p/E'_h) - \alpha(\bar{T}_{\text{hot}} - \bar{T}_{\text{cool}})]c_w(E'_w r_h/E'_h t_h)(r_h/h)[1/(1 + \chi)] \tag{A5b}$$

$$\bar{\varepsilon}_{\text{cool}} = \alpha\Delta T_c - [(1 - c_h)(r_h/t_h)(\Delta p/E'_h) - \alpha(\bar{T}_{\text{hot}} - \bar{T}_{\text{cool}})]c_w(E'_w r_h/E'_c t_c)(r_h/h)[1/(1 + \chi)] \tag{A5c}$$

where $\chi = \zeta/\eta_\infty$ and ζ and η_∞ are defined in Eq. (1d). The average elastic strains $\bar{\varepsilon}^{(e)}_{\text{wall}}$, etc., can be obtained from these results by subtracting out the average stress-free thermal strain, $\alpha\Delta T_h$ or $\alpha\Delta T_c$. The average stresses quoted in Eqs. (1a–1c) follow immediately from the relations $\bar{\sigma}_{\text{wall}} = E'_w\bar{\varepsilon}^{(e)}_{\text{wall}}$, etc.

The thermal strain gradient through the hot skin creates an additional thermal stress $\sigma_{\text{grad}T}$ at position z in the skin ($-t_h/2 < z < t_h/2$). If normal planes through the section remain normal to the hoop direction (no rotation of planes), then the thermal stress will be independent of x, vary linearly through the skin, and have the magnitude

$$\sigma_{\text{grad}T} = \alpha E'_h(T_1 - T_2)/2 \tag{A6}$$

on the surfaces. This stress contribution will be compressive on the hotter surface of the skin and tensile on the cooler surface.

Two further contributions to the stress state arise because the walls are discrete, which leads to additional bending moments in the hot skin. The gas pressure drop will generate a bending moment per unit width M_{P}, which will have a maximum value M_0 near a wall given approximately by

$$M_0 = \frac{(1 - c_h)\Delta P L^2}{12} \tag{A7}$$

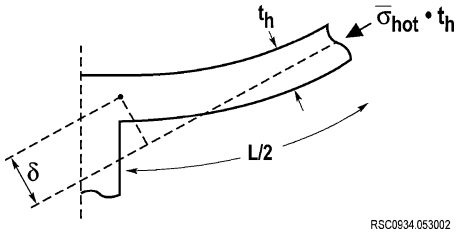

Fig. A2 Bending effect due to average stress in hot skin with radius of curvature r_h.

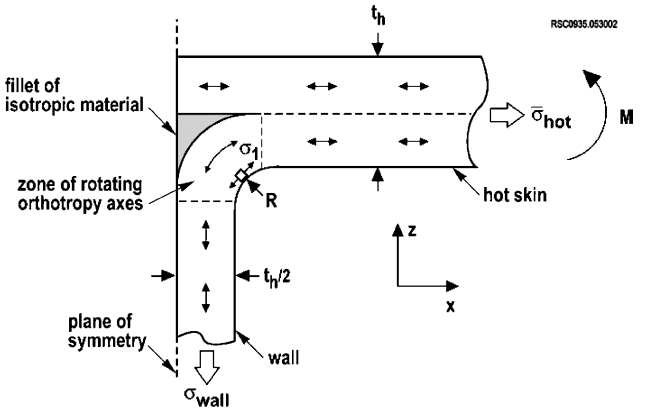

Fig. A3 Material model for finite element calculations of stress concentrations at junction between hot skin and wall; material piecewise homogeneous and orthotropic, with the direction corresponding to the locally dominant fiber direction indicated by arrows.

The maximum stress corresponding to the moment M_0 is given by

$$\sigma_{\text{bend}}^{(\Delta P)} = \left(6/t_h^2\right) M_0 \tag{A8}$$

and is also compressive on the hotter surface of the skin and tensile on the cooler surface. Because of the curvature of the hot skin, the average stress in the hot skin, $\bar{\sigma}_{\text{hot}}$, creates a bending moment that is also maximum at the skin wall junction (Fig. A2). The free-body diagram of Fig. A2 shows that this moment takes the value per unit width

$$\sigma_{\text{bend}}^{(T)} = 2t_h \delta \bar{\sigma}_{\text{hot}} \tag{A9a}$$

where

$$\delta = \tfrac{1}{8}(L^2/r_h) \tag{A9b}$$

Stress Concentration due to the Corner Geometry

Stress concentration effects due to the corner geometry were calculated by the FEM shown in Fig. A3. In the model, the material is assumed to be locally orthotropic everywhere, as expected for a fabric dominated by warp and weft fibers that locally are approximately straight. The dominant fiber directions (warp and weft in the woven fabric) are 1) into the plane of Fig. A3 and 2) as indicated by the arrows. These are assigned Young's moduli E_1 and E_2, respectively. The third direction is assigned Young's modulus E_3. Wedge-shaped elements around the radius of the junction represent a continuous variation of the axes of orthotropy. The fiber directions in the plane of the figure approximate the paths that plies might take if the junction were fabricated from two-dimensional plies. This is obviously an idealization of a three-dimensional architecture, but the results for stress concentration factors are nevertheless fair indicators of trends with geometry.

Two sets of calculations were performed for loads applied to the right end of the skin that would generate approximately uniaxial compression or pure bending in the skin not far from the junction. Unixaial compression represents the average stress $\bar{\sigma}_{\text{hot}}$ and the bending moment either the effects of the pressure drop ΔP or the temperature gradient, $T_1 - T_2$. Stress concentration factors, k_c and k_b, are defined for these two loads in terms of the component σ_1 of tensile or compressive stress that lies parallel to the local fiber direction (axis of orthotropy) at any point. The stress concentration factors represent the ratio of the maximum value of σ_1 to the maximum stress in the skin near but away from the junction. A third set of calculations was performed for a uniaxial stress $\bar{\sigma}_{\text{wall}}$, applied along the axis of the wall, balanced by shear tractions in the hot skin. A third stress concentration factor, k_w, defines the ratio of the maximum value of σ_1 to $\bar{\sigma}_{\text{wall}}$.

Table A1 Stress concentration factors for the skin/wall junction

$(E_2/E_1, E_3/E_1)$	R_c/t_h	$k_w = \sigma_1/\bar{\sigma}_{\text{wall}}$	$k_c = \sigma_1/\bar{\sigma}_{\text{hot}}$	$k_b = \sigma_1/\sigma_b$
(0.1, 1.0)	1/4	3.41	2.10	1.77
(0.5, 1.0)	1/4	2.91	2.12	1.78
(0.8, 1.0)	1/4	2.85	2.12	1.77
(0.1, 1.0)	1/8	4.36	2.31	1.98
(0.5, 1.0)	1/8	3.48	2.31	2.01
(0.8, 1.0)	1/8	3.34	2.31	2.01

The computed stress concentration factors are listed in Table A1 for different relative corner radii R_c/t_h and anisotropy ratios E_2/E_1 and E_3/E_1. The stress concentration factors k_c and k_b are never very far from 2, are quite insensitive to the degree of anisotropy, and only moderately sensitive to the radius of curvature. The concentration factor k_w is larger and depends more strongly on both the degree of anisotropy and the radius of curvature. Noting that the relative curvature is probably larger than one-quarter in thin-skinned integral structures and anisotropy is probably relatively mild, the bounds $k_c < 2$, $k_c < 1.7$, and $k_w < 3$ are reasonable design limits.

Appendix B: One-Dimensional Model of Heat Flow Through a Transpiring Skin

Consider the problem of a skin through whose upper and lower surfaces at $z = 0$ and $z = t$ are held at fixed, uniform temperatures T_2 and T_1, with $T_2 > T_1$. A coolant flows through a system of holes. Let R denote the ratio of the cross-sectional area of the holes at any position z within the skin to the area per unit length in z of the surface of the holes. Let h_1 denote the heat transfer coefficient for the hot surface and h_2 the heat transfer coefficient for the cool surface and the interior surfaces of the holes. Assume that the coolant has temperature T_c everywhere over the cool surface of the skin and is heated by heat transfer from the skin as it passes up through the holes. Assume that the temperature fields T_s and T_f in the skin and the fluid (coolant) are everywhere functions of z only. Let k_s denote the thermal conductivity of the skin in the z direction.

From considerations of heat flux conservation, one has

$$\frac{\mathrm{d}^2 T_s}{\mathrm{d}z^2} \frac{h_2}{k_s(1-R)}(T_s - T_f) = 0 \tag{B1}$$

$$\frac{\mathrm{d}T_f}{\mathrm{d}z} \frac{h_2}{R\rho_c c_p u}(T_s - T_f) = 0 \tag{B2}$$

where c_p is the heat capacity of the coolant, ρ_c is its density, and u is its velocity through the holes. From Eqs. (B1) and (B2)

$$(T_s - T_f)/T_c = A_1 \exp(\lambda_1 z/t) + A_2 \exp(\lambda_2 z/t) \tag{B3}$$

where A_1 and A_2 are constants to be determined by boundary conditions and λ_1 and λ_2 are given by

$$\lambda_{1,2} = \left\{ -\frac{t}{(1-R)} \frac{h_2}{\rho_c c_p u} \pm \sqrt{\left[\frac{t}{(1-R)} \frac{h_2}{\rho_c c_p u}\right]^2 + 4\frac{t}{R}\frac{h_2 t}{k_s}} \right\} \Big/ 2 \tag{B4}$$

The boundary conditions that can be used to determine A_1 and A_2 are

$$h_1(T_\infty - T_2) = h_2(T_1 - T_c) + \frac{1-R}{R}\rho_c c_p u(T_f[z=t] - T_c) \tag{B5a}$$

$$\left(\frac{\mathrm{d}T_s}{\mathrm{d}z}\right)_{z=t} = \frac{h_1}{k_s}(T_\infty - T_2) \tag{B5b}$$

$$A_1\lambda_1 + A_2\lambda_2 = \left(\frac{h_2 t}{k_s} - \frac{t}{1-R}\frac{h_2}{\rho_c c_p u}\right)\frac{T_1 - 1}{T_c} \tag{B5c}$$

The solution in terms of T_1, T_2, and $T_f|_{z=t}$ can be expressed in matrix form,

$$\begin{bmatrix} 1 & \frac{h_2}{h_1} & \frac{1-R}{R}\frac{\rho_c c_p u}{h_2} \\ \frac{h_1 t}{k_s} + C + F & -F + G & -F - C \\ \frac{\lambda_1 - \lambda_2}{e^{\lambda_1} - e^{\lambda_2}} & G + C - \frac{h_2 t}{k_s} & -\frac{\lambda_1 - \lambda_2}{e^{\lambda_1} - e^{\lambda_2}} \end{bmatrix} \begin{Bmatrix} T_2 \\ T_1 \\ T_f|_{z=t} \end{Bmatrix}$$

$$= \begin{Bmatrix} \frac{h_2}{h_1} + T_\infty \\ \frac{h_1 t}{k_s} T_\infty - F + G \\ C - \frac{h_2 t}{k_s} - G \end{Bmatrix} \tag{B6a}$$

with

$$C = \frac{t}{1-R}\frac{h_2}{\rho_c c_p u} \qquad F = \frac{\lambda_1 e^{\lambda_1} - \lambda_2 e^{\lambda_2}}{e^{\lambda_1} - e^{\lambda_2}} \qquad G = \frac{\lambda_2 e^{\lambda_1} - \lambda_1 e^{\lambda_2}}{e^{\lambda_1} - e^{\lambda_2}} \tag{B6b}$$

Results in the absence of transpiration holes follow by taking the limit $R \to 0$. Radiation flux Q_r on the hot surface can be included by modifying the boundary conditions (B5a) and (B5b).

Acknowledgments

The authors are pleased to acknowledge the generous support of the Air Force Office of Scientific Research for this work under Contract F49620-00-C-0023. Garry Brown of Princeton University was very helpful in associating the structural and materials ideas presented here with the combustion science and fluid mechanics of turbine engines.

References

[1]Davis, J. B., Marshall, D. B., Morgan, P. E. D., Oka, K. S., Barney, A. O., and Hogenson, P. A., "Damage Tolerant Thermal Protection Systems," *Proceedings of the Space 2000*, AIAA, Reston, VA, 2000.

[2]Cox, B. N., Marshall, D. B., Yang, Q. D., and Davis, J. B., "Integral Textile Ceramic Structures for Heat Exchanger Applications," *Proceedings of SAMPE 2003 Technical Conference*, SAMPE, Covina, Dayton, OH, 2003.

[3]Cox, B. N., Davis, J. B., Marshall, D. B., and Yang, Q. D., "Integral Textile Ceramic Composites for Turbine Engine Combustors," *Proceedings ASME Turbo Expo 2002*, American Society of Mechanical Engineers, Fairfield, NJ, 2002.

[4]Hsu, K.-Y., Goss, L. P., and Roquemore, W. M., "Characteristics of a Trapped-Vortex Combustor," *Journal of Propulsion and Power*, Vol. 14, No. 1, 1998, pp. 57–65.

[5]Morgan, P. E. D., and Marshall, D. B., "Ceramic Composites of Monazite and Alumina," *Journal of the American Ceramic Society*, Vol. 78, 1995, pp. 1553–63.

[6]Davis, J. B., Marshall, D. B., and Morgan, P. E. D., "Oxide Composites of Al_2O_3 and $LaPO_4$," *Journal of the European Ceramic Society*, Vol. 19, 1999, pp. 2421–2426.

[7]Davis, J. B., Marshall, D. B., and Morgan, P. E. D., "Monazite Containing Oxide–Oxide Composites," *Journal of the European Ceramic Society*, Vol. 20, No. 5, 2000, pp. 583–587.

[8]Keller, K. A., Mah, T.-I., Boakye, E. E., and Parthasarathy, T. A., "Gel-Casting and Reaction Bonding of Oxide–Oxide Minicomposites with Monazite Interphase," *Ceramic Engineering and Science Proceedings*, Vol. 21, No. 4, 2000, pp. 525–534.

[9]Parthasarathy, T. A., Boakeye, E., Cinibulk, M. K., and Perry, M. D., "Fabrication and Testing of Oxide/Oxide Microcomposites with Monazite and Hibonite as Interlayers," *Journal of the American Ceramic Society*, Vol. 82, No. 12, 1999, pp. 3575–3583.

[10]Hay, R. S., Boakye, E., and Petry, M. D., "Effect Of Coating Deposition Temperature On Monazite Coated Fiber," *Journal of the European Ceramic Society*, Vol. 20, No. 5, 1998, pp. 589–597.

[11]Boakye, E., Hay, R. S., and Petry, M. D., "Continuous Coating of Oxide Fiber Tows Using Liquid Precursors: Monazite Coatings On Nextel 720," *Journal of the American Ceramic Society*, Vol. 82, No. 9, 1999, pp. 2321–2331.

[12]Harrison, M. G., Millard, M. L., and Szweda, A., "Fiber Reinforced Ceramic Matrix Composite Member and Method for Making," U.S. Patent No. 5 306 554; U.K. Patent No. 2 230 259, 1994.

[13]Tu, W. C., Lange, F. F., and Evans, A. G., "Concept for a Damage-Tolerant Ceramic Composite with "Strong" Interfaces," *Journal of the American Ceramic Society*, Vol. 79, No. 2, 1996, pp. 417–424.

[14]Levi, C. G., Yang, J. Y., Dalgleish, B. J., Zok, F. W., and Evans, A. G., "Processing and Performance of an All-Oxide Ceramic Composite," *Journal of the American Ceramic Society*, Vol. 81, No. 8, 1998, pp. 2077–2086.

[15]Evans, A. G., Marshall, D. B., and Morgan, P. E. D., "Recent Advances in Oxide–Oxide Composite Technology," *Advanced Composite Materials*, Vol. 8, No. 1, 1999, pp. 17–23.

[16]Kramb, V. A., John, R., and Zawada, L. P., "Notched Fracture Behavior of an Oxide/Oxide Ceramic-Matrix Composite," *Journal of the American Ceramic Society*, Vol. 82, No. 11, 1999, pp. 3087–3096.

[17]Marshall, D. B., Morgan, P. E. D., Housley, R. M., and Cheung, J. T., "High Temperature Stability of the $Al_2O_3-LaPO_4$ System," *Journal of the American Ceramic Society*, Vol. 81, No. 4, 1998, pp. 951–56.

[18]Carelli, E., Fujita, H., Yang, J., and Zok, F. W., "Effects of Thermal Aging on the Mechanical Properties of a Porous-Matrix Ceramic Composite," *Journal of the American Ceramic Society*, Vol. 85, No. 3, 2002, pp. 595–602.

[19]Incropera, F. P., and DeWitt, D. P., *Introduction to Heat Transfer*, Wiley, New York, 1996.

[20]Lefebvre, A. H., *Gas Turbine Combustion*, Taylor and Francis, Philadelphia, 1998, Chap. 8.

[21]Touloukian, Y. S., and DeWitt, D. P., *Thermophysical Properties of Matter*, Vol. 8, *Thermal Radiative Properties, Nonmetallic Solids*, Plenum, New York, 1972.

[22]Ohki, T., Ikegaki, S., Kurasiki, K., Hamada, H., and Iwamoto, M., "Mechanical Properties of Flat Braided Composites with a Circular Hole," *Journal of Engineering Materials Technology*, Vol. 122, 2000, pp. 420–424.

[23]Mahomed, M., Carlson, C., Gu, P., and Sadler, R., "Effect of Machining on the Performance of Carbon/Epoxy 3D Woven Composites," *International Conference on Advanced Composite Materials*, edited by T. Chandra and A. K. Dhingra, 1993.

[24]Cox, B. N., Carter, W. C., and Fleck, N. A., "A Binary Model of Textile Composites: I Formulation," *Acta Metallurgica et Materialia*, Vol. 42, 1994, pp. 3463–3479.

[25]Xu, J., Cox, B. N., McGlockton, M. A., and Carter, W. C., "A Binary Model of Textile Composites: II Elastic Regime," *Acta Metallurgica et Materialia*, Vol. 43, 1995, pp. 3511–3524.

[26]Yang, Q. D., Rugg, K. L., and Cox, B. N., "Validated Predictions of the Local Variations of Strain in a 3D C/SiC Weave," *Journal of the American Ceramics Society*, In press.

[27]Yun, H. M., Gyekenyesi, J. Z., Chen, Y. L., Wheeler, D. R., and DiCarlo, J. A., "Tensile Behavior of SiC/SiC Composites Reinforced by Treated Sylramic SiC Fibers," *Ceramic Engineering and Science Proceedings*, Vol. 22, No. 3, 2001, pp. 521–531.

[28]Timoshenko, S. P., and Gere, J. M., *Theory of Elastic Instability*, 2nd ed., McGraw–Hill, New York, 1961.

[29]Crawford, M. E., Kay, W. M., and Moffat, R. J., "Full-Coverage Film Cooling," *Journal of Engineering for Power*, Vol. 102, 1980, pp. 1000–1006.

[30]Chen, F. J., Bowman W. J., and Bowersox, R., "Effects of Transpiration Cooling on Nozzle Heat Transfer," *Journal of Spacecraft and Rockets*, Vol. 33, 1996, pp. 453–455.

[31]Gladden, H. J., Yeh, F. C., and Fronek, D. L., "Heat Transfer Results and Operational Characteristics of the NASA Lewis Research Center Hot Section Cascade Test facility," *30th International Gas Turbine Conference and Exhibition*, American Society of Mechanical Engineers, New York, 1985.

[32]Koh, J. C. Y., Dutton, J. L., and Benson, B. A., "Fundamental Study of Transpiration Cooling," NASA CR-1345-23, 1973.

[33]Nealy, D. A., Mihelc, M. S., Hylton, L. D., and Gladden, H. J., "Measurement of Heat Transfer Distribution over the Surfaces of Highly Loaded Nozzle Guide Vane," *Journal of Engineering for Power*, Vol. 106, 1984, pp. 149–158.

[34]Camci, C., "An Experimental and Numerical Investigation of Heat Transfer Along the Suction Surface of a Film-Cooled Gas Turbine Blade," *Journal of Engineering for Gas Turbines and Power*, Vol. 107, 1989, pp. 991–1003.

[35]McNulty, J. C., Zok, F. W., Genin, G. M., and Evans, A. G., "Notch-Sensitivity of Fiber-Reinforced Ceramic-Matrix Composites: Effects of Inelastic Straining and Volume-Dependent Strength," *Journal of the American Ceramic Society*, Vol. 82, No. 5, 1999, pp. 1217–1228.

[36]Cox, B. N., Rugg, K. L., Berbon, M. Z., Marshall, D. B., Zok, F. W., He, M., and McMeeking, R. M., "Predictive Models for Textile Ceramic Matrix Composites at High Temperature," Rept. to Rocketdyne, Rockwell Scientific, Thousand Oaks, CA, 8 Feb. 2000.